

# Chemically Fueled Self-sorted Hydrogels

*Nishant Singh,<sup>±\*</sup> Alvaro Lopez-Acosta,<sup>±</sup> Georges J.M. Formon, Thomas M. Hermans\**

**Address:** Université de Strasbourg, CNRS, UMR7140, 4 Rue Blaise Pascal, 67081 Strasbourg, France E-mail: [nishant.singh@unistra.fr](mailto:nishant.singh@unistra.fr), [hermans@unistra.fr](mailto:hermans@unistra.fr)

**Keywords:** chemical fuels, self-sorting, hydrogels, secondary nucleation, multicomponent systems.

**Abstract:** Narcissistic self-sorting in supramolecular assemblies can help to construct materials with more complex hierarchies. Whereas controlled changes in pH or temperature have been used to this extent for two-component self-sorted gels, here we show that a chemically fueled approach can provide three-component materials with high precision. The latter materials have interesting mechanical properties, such as enhanced or suppressed stiffness, and intricate multi-step gelation kinetics. In addition, we show that we can achieve supramolecular templating, where pre-existing supramolecular fibers first act as a templates for growth of a second gelator, after which they can selectively be removed.

## 1. Introduction

Narcissistically self-sorted hydrogels have been made by methods like rapid mixing of components,<sup>1</sup> solvent switching,<sup>2</sup> chiral recognition,<sup>3</sup> electrostatic interactions,<sup>4</sup> pH change,<sup>5,6</sup> and supramolecular catalysis.<sup>5,6</sup> Thermal annealing is most commonly used, where different gelation temperatures of the molecules allow them to self-assemble sequentially.<sup>7-10</sup> A second approach, uses a gradual change in pH to create two-component self-sorted hydrogels. Gluconolactone (GdL) hydrolysis leads to sequential gelation of co-dissolved monomers at their respective  $pK_a$  values, leading to materials with improved mechanical, optoelectronic, and photoconductive properties.<sup>11-19</sup>

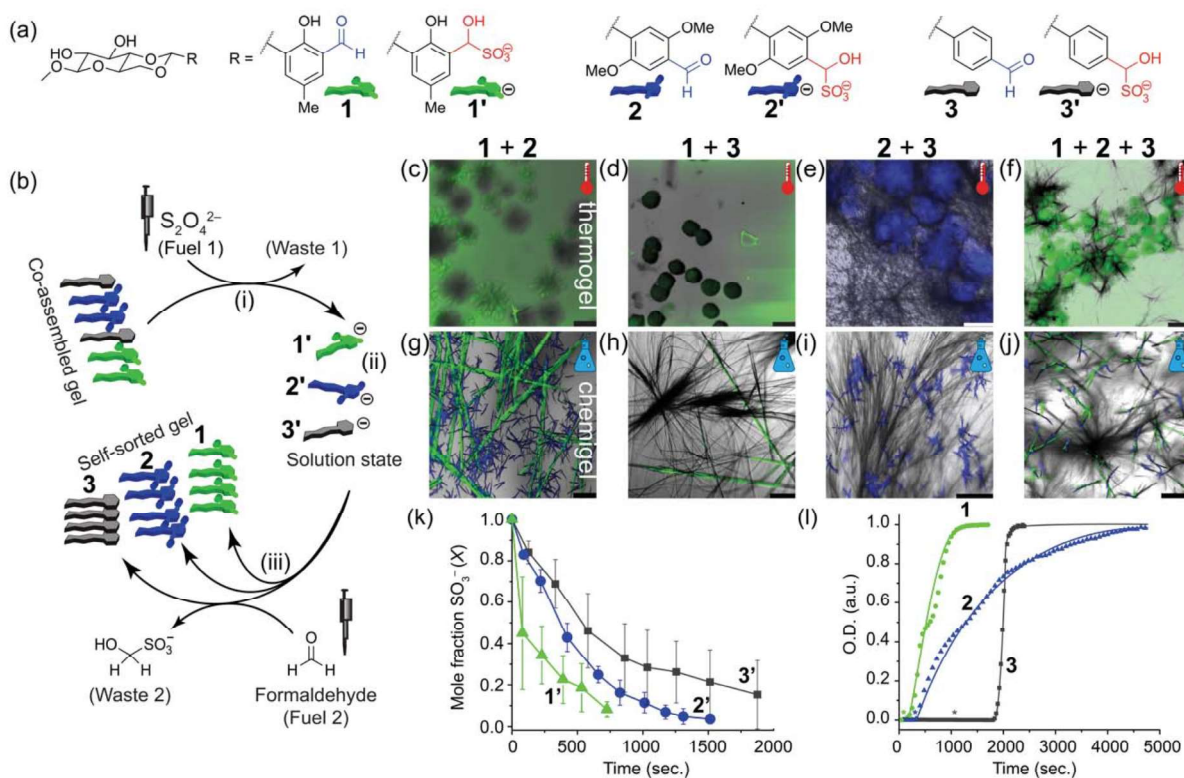
26 van Esch and co-workers have shown fabrication of self-sorted hydrogels using ‘kinetic self-  
27 sorting’ of both a charged and neutral hydrogelator which form *in situ* via hydrazone formation.  
28 The reaction kinetics of the hydrogelators were found to be comparable, but they could still  
29 self-sort in certain cases due to their differing minimum gelation concentrations.<sup>20</sup>  
30 Here we show that a chemically fueled functional group transformation—that is, aldehyde-to-  
31 hydroxysulfonate (and back)—can lead to exquisite control over self-sorting, providing access  
32 to well-structured three-component hydrogels. This approach is useful, since chemically very  
33 similar gelators with different innate reactivity can be used, which would otherwise co-  
34 assemble when using controlled cooling. Moreover, since the functional group transformation  
35 is reversible, we can achieve supramolecular templating, where first a self-assembled fiber  
36 guides the growth of a second, after which the first can be selectively removed. Overall, we  
37 believe chemically fueled approaches are promising to get more exquisite control over  
38 supramolecular structures and the mechanical properties of multi-component gels.

39

## 40 **2. Results and discussion**

41 We recently reported a chemically fueled reaction cycle capable of gel-sol-gel transitions using  
42 aldehyde-containing saccharide derivative (compound **3** in Figure 1a).<sup>21</sup> In the latter, a  
43 thermally annealed hydrogel of **3** was first disassembled using sodium dithionite DT by  
44 converting the aldehyde moiety into its water-soluble hydroxysulfonate analog **3'**.  
45 Formaldehyde (HCHO), produced *in situ* with a time-delay, then converted sulfonate **3'** back  
46 to aldehyde **3**, again leading to gelation.

47 In the current work, we synthesized compounds **1** and **2** with close structural similarity to **3** and  
48 studied their assembly behavior in heat-cool cycles and their response to chemical fuels, both  
49 for the pure compounds and that of their mixtures (Figure 1). Surprisingly, this led to up to  
50 three-component well-structured self-sorted hydrogels.



51

52 **Figure 1: Self-sorting achieved by a chemical fuel.** (a) Chemical structures of the used  
 53 gelators, and their hydroxysulfonate analogs (numbers with prime indication). (b) Scheme  
 54 starting from a co-assembled thermogel that is disassembled by fuel 1 (i), resulting in a solution  
 55 state (ii). After addition of fuel 2 (iii) a self-sorted gel is formed. (c–j) Confocal images of  
 56 thermally annealed (c–f), or chemically fueled (g–j) assemblies. (k) Kinetics of consumption  
 57 of **1'**, **2'**, and **3'** (21.6 mM) after HCHO (~44 eq.) addition from <sup>1</sup>H-NMR. (l) Self-assembly  
 58 kinetics from turbidity measurements at 500 nm using UV-Vis spectroscopy (see Figure S9 for  
 59 detailed concentration dependent measurements). Assemblies of **1**, **2**, and **3** (21.6 mM) from **1'**,  
 60 **2'**, and **3'** upon addition of HCHO (47 eq.). Lines to guide the eye. Lag phases are indicated  
 61 with asterisks.

62  
63

64

## 65 **Thermally annealed ‘thermogels’**

66 We started from the traditional ‘controlled cooling’ approach<sup>7-10</sup> to try and obtain self-sorted  
67 hydrogels. Both pure **1** as well as **2** formed free standing hydrogels by thermal annealing with  
68 critical gelation concentration (CGC) of 23.5 mM and 21.6 mM, respectively. As a reminder,  
69 we had previously shown that thermogel **3** had a CGC of 25.8 mM.<sup>[21]</sup> Such ‘thermogels’ have  
70 gelation temperatures ( $T_{\text{gel}}$  at 35 mM) of 74°C for **1**, 78°C for **2**, and 60°C for **3**, as described  
71 in SI section S3.1. Confocal laser scanning microscopy (CLSM, including transmitted light  
72 imaging) showed that thermogel **1** (35 mM) formed a bimodal distribution of green fluorescent  
73 fibers: small fibers of width  $< 1 \mu\text{m}$  and length  $\sim 200 \mu\text{m}$ , and long fibers of width  $\sim 10 \mu\text{m}$  and  
74 length  $> 500 \mu\text{m}$ . The latter were also much more emissive as compared to the short fibers.  
75 Thermogels of **2** showed large  $\sim 400 \mu\text{m}$  blue fluorescent spherulites while **3** formed thin (1–2  
76  $\mu\text{m}$ ) and long ( $> 1000 \mu\text{m}$ ) non-fluorescent fibers (SI Figure **S1**). Next, we tested thermally  
77 annealed two- and three-components combinations of these molecules (total concentration is  
78 always constant at 35 mM). Thermogel **1+2** (ratio 0.5 : 0.5) formed a free-standing hydrogel  
79 composed of co-assembled spherules (Figure 1c) with an intermediate emission wavelength  
80  $\lambda_{\text{em}} = 523 \text{ nm}$ , as compared to the pure assemblies that were 548 and 485 nm, respectively. The  
81 latter suggests that **1** and **2** co-assemble,<sup>22</sup> when thermally cycled. In addition, the fibrous  
82 structure of **1** was completely suppressed in the **1+2** gel, further supporting co-assembly.  
83 **Thermogel 1+3** only formed spherical co-assembled aggregates (Figure 1d), whereas pure **1**  
84 and **3** both form long fibers. The fluorescence emission wavelength is identical to that of **1**,  
85 since **3** is non-emissive. In addition, gelation was suppressed, whereas pure **1** and **3** both form  
86 gels at 35 mM at room temperature. This shows that co-assembly can be detrimental for heat–  
87 cool thermogels. The combination of **2+3** formed self-sorted hydrogels (Figure 1e), where the  
88 characteristic features of pure **2** and **3**—being blue spherulites and non-emissive fibers,  
89 respectively (cf. Figure **S1**)—can be recognized. The latter makes sense, as **3** has a  $T_{\text{gel}}$  that is  
90 18 degrees lower than that of **2**. Therefore, during cooling from 85°C to room temperature, first

91 **2** has time to form, followed by **3** later on. The same argumentation, however, does not hold  
92 for **1+3**, which have gelation temperatures that are 14 degrees apart, but still co-assemble.  
93 Clearly, predicting narcissistic self-sorting in structurally similar molecules at equilibrium is  
94 not straightforward. Three-component mixtures of **1+2+3** (ratio: 0.2/0.2/0.6 and 0.33/0.33/0.33)  
95 showed features of co-assembled spherical **1+2**, and some fibrous **3** albeit much shorter than in  
96 pure **3** (Figure 1e). Overall, multicomponent thermogels were mostly unable to self-sort except  
97 for the combination **2+3**. Instead, co-assembly was preferred, leading to loss of their fibrillar  
98 morphology and in select cases their gel-forming ability.

99

## 100 Chemically fueled ‘chemigels’

101 We now move to chemically fueled gels or ‘chemigels’ as we will refer to them. Typically, ~6  
102 equivalents of DT were added to a previously formed thermogel, leading to chemical  
103 conversion of the aldehyde moiety to a hydroxysulfonate (i.e., **1'**, **2'**, or **3'**), which resulted in  
104 complete dissolution. After 21 hours to ensure full disassembly and dissolution, HCHO was  
105 added to revert the hydroxysulfonate back to the aldehyde inducing re-assembly.

106 Looking first at pure chemigels, we see that **1** still forms green emissive fibers as compared to  
107 the thermogel. However, they are not bi-modal in size distribution, but instead more uniform  
108 and straight. Compound **2** is also still forming spherulites, but they are 20 times smaller (at 20–  
109 30  $\mu\text{m}$ ) as compared to the thermally annealed case (cf. Figure S4). The latter indicates that  
110 there are more frequent nucleation events when chemically fueled. And lastly, compound **3**  
111 forms non-emissive long fibers both in the thermogels and chemigels (see Figure S13 for  
112 fluorescence emission data). Thermally, the fibers are randomly distributed in space  
113 (homogeneous nucleation), whereas chemically they grow more from defined nucleation  
114 centers into fractal-like structures, due to secondary nucleation as we showed previously.<sup>21</sup>

115 For multicomponent systems, **1'**, **2'**, and **3'** were mixed when fully disassembled, followed by  
116 addition of HCHO to form the multicomponent chemigels. That is, no heating or cooling

117 procedures were involved to make chemigels. Strikingly, all multicomponent chemigels give  
118 rise to self-sorted assemblies (see Figure 1g–j), whereas this was only the case for **2+3** thermally.  
119 Even the **1+2+3** chemigel is self-sorted into the three characteristic green/blue/black (non-  
120 emissive) colors.

121 Upon closer inspection, there is another interesting change in the assembly process of **2**. Instead  
122 of self-nucleating and forming blue spherulites (cf. Figure S4), it grows on top of green fibers  
123 of compound **1**, if present. That is, heterogenous nucleation of **2**, using assemblies of **1** as  
124 nucleation sites, is more favorable than homogeneous nucleation. The result is that green fibers  
125 are formed, which have blue protrusions from its sides (Figure 1g, SI Figure S5, SI Movie 1  
126 and 2). Compound **2**, however, does not perform a heterogeneous nucleation on top of **3** (see  
127 Figure S5), likely because their chemical structures are too different from each other, favoring  
128 full narcissistic self-sorting. Overall, excellent self-sorting behavior is achieved using our  
129 chemically fueled (HCHO) approach. To understand why this is the case, we have examined  
130 the chemical and self-assembly kinetics of each building block, which is described next.

131

### 132 **Chemical reactivity**

133 The rate at which the individual hydroxysulfonates revert back to their respective aldehydes  
134 was determined by time-dependent <sup>1</sup>H NMR kinetics (Figure 1k). The rates of hydroxysulfonate  
135 consumption were found to be **1' > 2' > 3'**, which may be explained by looking at their chemical  
136 structures. Namely, compounds **1** and **2** have electron donating groups: **1** has ortho-hydroxyl  
137 and meta-methyl substituents, and **2** has two methoxy groups at the ortho and meta positions.  
138 These substituents cause **1'** and **2'** to react faster with HCHO to form their corresponding  
139 aldehydes as compared to **3'→3**.<sup>23</sup> Moreover, the –OH group next to the –CHO can further  
140 stabilize **1** as a product through intra-molecular hydrogen bonding and thus further accelerate  
141 its hydroxysulfonate to aldehyde conversion<sup>24–26,31</sup> (as confirmed by NMR, see SI Figure S12).

142 Thus, the overall rates of reaction  $1 > 2 > 3$  are reasonable considering their aromatic  
143 substitution patterns.

144

#### 145 **Cooperative self-assembly for all derivatives**

146 Once  $1'-3'$  has been chemically converted to its aldehyde form  $1-3$ , it is charge neutral and can  
147 start assembling. The assembly kinetics were followed by UV-Vis turbidity measurements,  
148 where the optical density (O.D.) at 500 nm was tracked after addition of a large excess ( $\sim 47$   
149 equivalents) of HCHO to hydroxysulfonate solutions (Figure 1h).

150 UV-Vis turbidity measurements show that a cooperative mechanism of self-assembly for all  
151 three systems is present. Specifically, a lag time is observed for  $1-3$  (Figure 11), and adding  
152 pre-formed self-assembled seeds leads to immediate growth without a lag phase (Figure S9).

153 The kinetic time traces, however, show evidence of biphasic behavior and are not accurate  
154 enough to be analyzed by available nucleation / elongation / fragmentation models.<sup>27</sup>

155 Corresponding to the rate of hydroxysulfonate consumption by NMR studies, the rate of self-  
156 assembly obtained by UV-Vis measurements and kinetic fitting gave the order of assembly as

157  $1 > 2 > 3$  (Figure 11, Figure S9, and section 3.6 of SI). Overall,  $1$  aggregates faster, followed by  
158  $2$ , and  $3$  has the slowest assembly kinetics. This is evidenced by a rate constant for primary

159 nucleation ( $k_n$ ) 10 orders of magnitude smaller for  $3$  when compared to  $1$  and  $2$  (which have  
160 values in the same order of magnitude). After nucleation, aggregates of  $1$  grow faster than  $2$

161 due to a  $\sim 2.3$  times higher elongation rate constant ( $k_p$ ) and the presence of secondary nucleation  
162 that is not observed in the aggregation of  $2$  and is only important after nucleation. Confocal

163 images and videos further confirmed this order of assembly in multicomponent mixtures  
164 forming self-sorted structures (SI Figure S7, SI Movie 1, 2, 3).

165

166

167

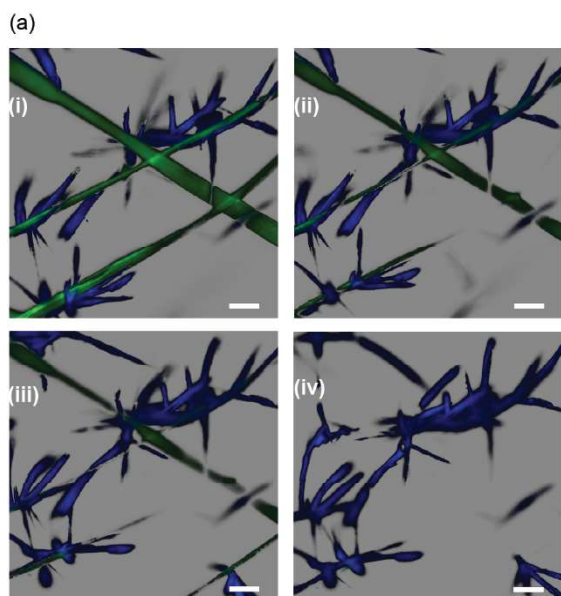
168

169

170 **Selective supramolecular template removal**

171  
172 As shown above in Figure 1g, compound **2** can grow on top of assemblies of compound **1** due  
173 to heterogeneous nucleation, leading to **1+2** structures. Interestingly, we found that upon  
174 addition of DT to **1+2** structures, we could selectively remove **1** (see disappearance of green **1**  
175 fibers in Figure 2a; see also SI Figure S8, SI Movie 4). Considering their reactivity—where the  
176 rate of  $1' \rightarrow 1$  was faster than  $2' \rightarrow 2$  (Figure 1g)—we had expected that  $2 \rightarrow 2'$  would be faster  
177 than  $1 \rightarrow 1'$ . However, the reverse is observed, and **1** that forms first upon addition of HCHO  
178 (see Figure S8), also disappears first when adding DT.

179



185  
186  
187  
188

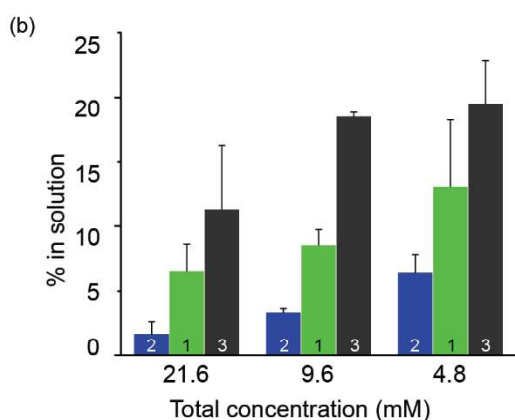


**Figure 2: Solubility differences allow for selective supramolecular template removal.** (a) Confocal microscopy time-lapse images showing selective removal of green scaffold (**1**) by slow addition of sodium dithionite DT while keeping the blue fluorescent assemblies of **2** intact. Scale bars: 50  $\mu\text{m}$ , time interval between images i–iv: 20 min. (b) Percentage of soluble molecules as a function of total solution concentration of individual assemblies of **1–3**, determined by  $^1\text{H}$  NMR in comparison with a soluble internal standard (hydroquinone).

180

181

182

183

184



189 It is not entirely fair to make such simple assumptions based on chemical reactivity considering  
190 electron donating groups. In fact, when measuring the conversion rates of  $1' \rightarrow 1$  and  $2' \rightarrow 2$  we  
191 are starting from completely homogenous and monomeric hydroxysulfonates that react with  
192 HCHO. When viewing the conversion of  $1 \rightarrow 1'$  and  $2 \rightarrow 2'$ , we start in the assembled state with  
193 micrometer-sized structures. It takes time for the DT to penetrate and react with structures of  
194 these sizes. However, DT can react more quickly with species that are in their monomeric state.  
195 NMR studies showed a higher proportion of soluble molecules for **1** than **2** (Figure 2b), due to  
196 their solubilizing hydroxyl groups. We therefore think that DT reacts preferentially with soluble  
197 **1** molecules, and therefore induces the selective **disassembly** of **1** fibers, as we have observed  
198 experimentally. That is, a depletion of **1** monomers below the critical aggregation concentration,  
199 causes **1** molecules to be extracted from **1** fibers. In effect, **1** fibers act a removable  
200 supramolecular template for the growth of **2** structures. We could confirm the latter hypothesis  
201 using NMR by treating chemically fueled assemblies of **1** with different DT concentrations. DT  
202 when below the net concentration of HCHO+**1** (soluble monomers) did not lead to  $1'$ , and was  
203 preferentially consumed by excess HCHO. At concentrations comparable to HCHO+**1** (soluble  
204 monomers) we could observe quick conversion of soluble **1** monomers to  $1'$ . Once the DT was  
205 consumed, we observed monomers of **1** reappearing in the solution along with  $1'$  due to  
206 dissolution of the aggregates. At much higher concentration of DT all the molecules of **1**  
207 (soluble+aggregates) were quickly converted to  $1'$  (SI section 3.7, SI Figure **S12**).

208

209

210

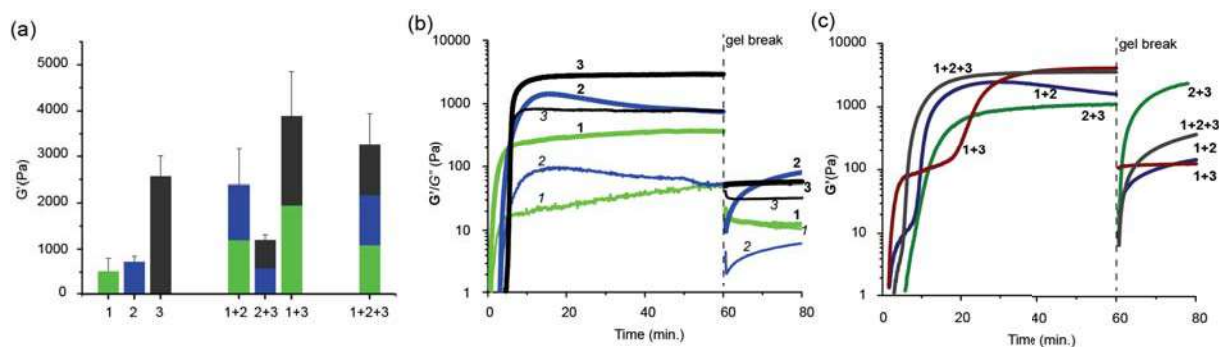
211

212

213

214

## 215 Mechanical properties of multi-component gels



216  
 217 **Figure 3: Mechanical characterization of chemically fueled multicomponent gels.** (a)  
 218 Storage moduli ( $G'$ ) of one, two, and three component chemically-fueled self-sorted hydrogels.  
 219 (b) Time-evolution of hydrogels after adding HCHO to hydroxysulfonate **1'**, **2'**, or **3'** solutions.  
 220 Gel breaking (dashed vertical line) was performed by applying a high shear rate ( $1000\text{ s}^{-1}$ ) at  
 221 60 min. (c) The same as panel b but for two, and three component mixtures.

222  
 223 The mechanical properties of single and multicomponent self-sorted hydrogels were evaluated  
 224 by rheology (Figure 3, see triplicate runs in Figure S10). To this end, solutions of **1'**, **2'**, or **3'**  
 225 or mixtures of the latter three always at a total concentration of 35 mM, were quickly mixed  
 226 with an excess of HCHO and placed between the parallel plates of the rheometer (see Section  
 227 3.8 of the SI). Compound **1** formed unstable hydrogels that expelled solvent under slight  
 228 perturbation (ca. 500 Pa) probably because its rigid crystalline fibers could not percolate solvent  
 229 properly. Hydrogels of **2** evolved quickly to reach a high  $G'$  (ca. 2000 Pa) but eventually  
 230 stabilized to lower values (ca. 700 Pa). The latter can be seen in Figure 3b, where a maximum  
 231 in  $G'$  and  $G''$  was reached around 17 minutes, after which both decrease and reach a plateau.  
 232 This behavior can be due to quick formation of numerous small assemblies (see SI Figure S4),  
 233 but in the longer run, absence of long fibers would result in partial sedimentation of the  
 234 assemblies to give the final  $G'$  values. Hydrogels of **3** had the best mechanical response (see  
 235 black bar in Figure 3a and black lines in panel b), forming the stiffest of the three materials due  
 236 to their long wavy fibers that are typically seen in supramolecular hydrogels. Interestingly,  
 237 hydrogels consisting of **1+2** structures—formed by secondary nucleation of **2** on **1**—had  
 238 significantly higher mechanical strength (ca. 2300 Pa) than either **1** or **2** alone (Figure 3a,c). In  
 239 contrast, solvent expulsion (for **1** alone) or settling of aggregates (for **2** alone) was not observed.

240 Instead, the blue branches of **2** on fibers of **1**, seem to give rise to better entanglement and thus  
241 the formation of a more stable hydrogel. Another interesting feature, was the step-wise  
242 evolution of  $G'$  for **1+3** self-sorted gels (red line in Figure 3c). From microscopy we know that  
243 **1** forms first, followed by **3** that is the slowest to nucleate (see Figure S7d and SI Movie 3).  
244 Interestingly, the total  $G'$  of **1+3** is  $\sim 50\%$  higher than that of **3** alone, at just half the  
245 concentration of **3**. The high mechanical strength can be attributed to the presence of long  
246 extended fiber networks from both the individual components where the second network fills  
247 in the empty spaces to create a more densely packed hydrogel. In contrast, the **2+3** combination  
248 formed hydrogels with a lower mechanical strength (1200 Pa) than pure **3**, but slightly above  
249 that of pure **2** (Figure 3a,c). The three component system (**1/2/3** in ratio 0.33/0.33/0.33) was  
250 comparable to **1+3** gels.

251 The ability of these gels to self-heal after applying a high shear rate ( $1000\text{ s}^{-1}$ ) for 30 seconds  
252 was also evaluated. Hydrogels of **1**, once sheared, could not recover ( $G' \approx G'' \approx 10\text{ Pa}$ ) and  
253 separation of solvent from fibers was observed. Further, gels of **2** could only partially recover  
254 to about 10% of their initial  $G'$ . The long fibers of **3** somewhat resisted total disruption of the  
255 gel properties, but the self-healing only recovered  $\sim 4\%$  of the initial  $G'$ . Similarly poor  
256 recovery after shear damage was observed for **1+2** and **1+2+3**, whereas **1+3** did not show any  
257 recovery. In sharp contrast, **2+3** could recover and form gels that were stronger even than the  
258 initial self-sorted **2+3** gels. Apparently, the **2+3** gel shows a synergistic interaction between  
259 fibers of **3** and spherulites of **2**. The latter synergy presents intriguing prospects for other  
260 multicomponent self-sorted gels and materials, which can have materials properties—such as  
261 self-healing—that are not observed in the respective single component materials.

262

### 263 3. Conclusions and outlook

264 We showed how chemical fuels can be used to construct multicomponent self-sorted hydrogels.  
265 Subtle differences in the chemical structure of the hydrogelators affected both their reactivity  
266 toward the chemical fuels, as well as their propensity to self-assemble. The result is that intricate  
267 self-sorted materials could be made of molecules that using traditional approaches (e.g.,  
268 heat/cool) would form poorly ordered co-assemblies. Our approach even allows for  
269 supramolecular templates to be used. That is, a first assembly guides the second, after which  
270 the first can selectively remove.

271 Man-made chemically fueled systems have already shown fascinating properties such as  
272 oscillations,<sup>28</sup> dynamic vesicles,<sup>29</sup> and transient assemblies<sup>21,30,31</sup>, but have not been applied to  
273 control the hierarchy of multicomponent systems. Although ATP-powered transiently self-  
274 sorted colloids have been shown using DNA building blocks,<sup>32</sup> a similar approach in chemically  
275 fueled synthetic materials was lacking. We believe chemically fueled self-sorting provides a  
276 new method to achieve complex functional materials consisting of programmed orthogonal  
277 networks.

278

### 279 Acknowledgements.

280 N.S. would like to acknowledge Marie Curie Individual fellowship EU project 890659-  
281 CYCLOTUBES for funding. A.L-A. would like to acknowledge European Union's Horizon  
282 2020 research and innovation programme under the Marie Skłodowska-Curie grant agreement  
283 no. 812868 for PhD funding. G.J.M.F. received funding from Ministère de l'Éducation  
284 Nationale de l'Enseignement supérieur et de la Recherche. T.M.H would like to acknowledge  
285 funding from ERC-2017-STG "Life-Cycle" (757910). We would like to thank Cyril  
286 Antheaume for his help with all the NMR and mass experiments. **N.S. and A.L-A. contributed**  
287 **equally to the work. \* N.S. and T.M.H. are corresponding authors.**

288 **ASSOCIATED CONTENT**

289 **Supporting Information.**

290 The Supporting Information is available free of charge.

291 Materials, methods, synthesis, characterization, additional data, and modeling information ([PDF](#))

292 Movie 1, confocal microscopy showing sequential formation of 1+2+3, 3 component hydrogel  
293 ([MP4](#))

294 Movie 2, confocal microscopy showing sequential formation of compounds 1+2, 2 component  
295 hydrogel ([MP4](#))

296 Movie 3, confocal microscopy showing sequential formation of compounds 1+3, 2 component  
297 hydrogel ([MP4](#))

298 Movie 4, confocal microscopy showing selective template removal of 1 from 1+2 hybrid structures  
299 ([MP4](#)).

300

301 **AUTHOR INFORMATION**

302 **Corresponding Authors**

303 Nishant Singh – Université de Strasbourg, CNRS, UMR7140, 4 Rue Blaise Pascal, 67081  
304 Strasbourg, France; Email : nishant.singh@unistra.fr

305 Thomas M. Hermans – Université de Strasbourg, CNRS, UMR7140, 4 Rue Blaise Pascal, 67081  
306 Strasbourg, France

307

308 **Authors**

309 Alvaro Lopez-Acosta – Université de Strasbourg, CNRS, UMR7140, 4 Rue Blaise Pascal,  
310 67081 Strasbourg, France;

311 Georges J.M. Formon – Université de Strasbourg, CNRS, UMR7140, 4 Rue Blaise Pascal,  
312 67081 Strasbourg, France;

313

314

315

316 Received: ((will be filled in by the editorial staff))

317 Revised: ((will be filled in by the editorial staff))

318 Published online: ((will be filled in by the editorial staff))

319

320 **References:**

- 321 1. Sun, Y.; Bentolila, L. A.; Deming, T. J., Self-Sorting Microscale Compartmentalized Block Copolypeptide  
322 Hydrogels. *ACS Macro Letters* **2019**, *8* (10), 1275-1279.
- 323 2. Chen, H.; Huang, C.; Deng, Y.; Sun, Q.; Zhang, Q.-L.; Zhu, B.-X.; Ni, X.-L., Solvent-Switched Schiff-  
324 Base Macrocycles: Self-Sorting and Self-Assembly-Dependent Unconventional Organic Particles. *ACS Nano*  
325 **2019**, *13* (3), 2840-2848.
- 326 3. He, H.; Zheng, H.; Ma, M.; Shi, Y.; Gao, Z.; Chen, S.; Wang, X., Chirality on dendrimers: “roll booster”  
327 of the molecule-level self-sorting assembly in two-component supramolecular gel system. *Chemical*  
328 *Communications* **2020**, *56* (20), 2983-2986.
- 329 4. Sahoo, J. K.; VandenBerg, M. A.; Ruiz Bello, E. E.; Nazareth, C. D.; Webber, M. J., Electrostatic-driven  
330 self-sorting and nanostructure speciation in self-assembling tetrapeptides. *Nanoscale* **2019**, *11* (35), 16534-  
331 16543.
- 332 5. Panja, S.; Dietrich, B.; Shebanova, O.; Smith, A. J.; Adams, D. J., Programming Gels Over a Wide pH  
333 Range Using Multicomponent Systems. *Angewandte Chemie International Edition* **2021**, *60* (18), 9973-9977.
- 334 6. Singh, N.; Maity, C.; Zhang, K.; Angulo-Pachón, C. A.; van Esch, J. H.; Eelkema, R.; Escuder, B.,  
335 Synthesis of a Double-Network Supramolecular Hydrogel by Having One Network Catalyse the Formation  
336 of the Second. *Chemistry – A European Journal* **2017**, *23* (9), 2018-2021.

- 337 7. Smith, M. M.; Smith, D. K., Self-sorting multi-gelator gels—mixing and ageing effects in thermally  
338 addressable supramolecular soft nanomaterials. *Soft Matter* **2011**, *7* (10), 4856-4860.
- 339 8. Moffat, J. R.; Smith, D. K., Controlled self-sorting in the assembly of ‘multi-gelator’ gels. *Chemical*  
340 *Communications* **2009**, (3), 316-318.
- 341 9. Singh, N.; Zhang, K.; Angulo-Pachón, C. A.; Mendes, E.; van Esch, J. H.; Escuder, B., Tandem reactions  
342 in self-sorted catalytic molecular hydrogels. *Chemical Science* **2016**, *7* (8), 5568-5572.
- 343 10. Singh, N.; Escuder, B., Competition versus Cooperation in Catalytic Hydrogelators for anti-Selective  
344 Mannich Reaction. *Chemistry – A European Journal* **2017**, *23* (41), 9946-9951.
- 345 11. Draper, E. R.; Eden, E. G. B.; McDonald, T. O.; Adams, D. J., Spatially resolved multicomponent gels.  
346 *Nature Chemistry* **2015**, *7* (10), 848-852.
- 347 12. Draper, E. R.; Adams, D. J., Low-Molecular-Weight Gels: The State of the Art. *Chem* **2017**, *3* (3), 390-410.
- 348 13. Castilla, A. M.; Draper, E. R.; Nolan, M. C.; Brasnett, C.; Seddon, A.; Mears, L. L. E.; Cowieson, N.;  
349 Adams, D. J., Self-sorted Oligophenylvinylene and Perylene Bisimide Hydrogels. *Scientific Reports* **2017**, *7*  
350 (1), 8380.
- 351 14. Morris, K. L.; Chen, L.; Raeburn, J.; Sellick, O. R.; Cotanda, P.; Paul, A.; Griffiths, P. C.; King, S. M.;  
352 O’Reilly, R. K.; Serpell, L. C.; Adams, D. J., Chemically programmed self-sorting of gelator networks.  
353 *Nature Communications* **2013**, *4* (1), 1480.
- 354 15. Draper, E. R.; Lee, J. R.; Wallace, M.; Jäckel, F.; Cowan, A. J.; Adams, D. J., Self-sorted photoconductive  
355 xerogels. *Chemical Science* **2016**, *7* (10), 6499-6505.
- 356 16. Draper, E. R.; Dietrich, B.; Adams, D. J., Self-assembly, self-sorting, and electronic properties of a  
357 diketopyrrolopyrrole hydrogelator. *Chemical Communications* **2017**, *53* (11), 1864-1867.
- 358 17. Cross, E. R.; Sproules, S.; Schweins, R.; Draper, E. R.; Adams, D. J., Controlled Tuning of the Properties  
359 in Optoelectronic Self-Sorted Gels. *Journal of the American Chemical Society* **2018**, *140* (28), 8667-8670.
- 360 18. Piras, C. C.; Smith, D. K., Sequential Assembly of Mutually Interactive Supramolecular Hydrogels and  
361 Fabrication of Multi-Domain Materials. *Chemistry – A European Journal* **2019**, *25* (48), 11318-11326.
- 362 19. Okesola, B. O.; Wu, Y.; Derkus, B.; Gani, S.; Wu, D.; Knani, D.; Smith, D. K.; Adams, D. J.; Mata, A.,  
363 Supramolecular Self-Assembly To Control Structural and Biological Properties of Multicomponent  
364 Hydrogels. *Chemistry of Materials* **2019**, *31* (19), 7883-7897.
- 365 20. Choi, S.; Mukhopadhyay, R. D.; Kim, Y.; Hwang, I.-C.; Hwang, W.; Ghosh, S. K.; Baek, K.; Kim, K.,  
366 Fuel-Driven Transient Crystallization of a Cucurbit[8]uril-Based Host–Guest Complex. *Angewandte Chemie*  
367 *International Edition* **2019**, *58* (47), 16850-16853.
- 368 21. Singh, N.; Lainer, B.; Formon, G. J. M.; De Piccoli, S.; Hermans, T. M., Re-programming Hydrogel  
369 Properties Using a Fuel-Driven Reaction Cycle. *Journal of the American Chemical Society* **2020**, *142* (9),  
370 4083-4087.
- 371 22. Albertazzi, L.; van der Zwaag, D.; Leenders Christianus, M. A.; Fitzner, R.; van der Hofstad Remco, W.;  
372 Meijer, E. W., Probing Exchange Pathways in One-Dimensional Aggregates with Super-Resolution  
373 Microscopy. *Science* **2014**, *344* (6183), 491-495.
- 374 23. Hammett, L. P., The Effect of Structure upon the Reactions of Organic Compounds. Benzene Derivatives.  
375 *Journal of the American Chemical Society* **1937**, *59* (1), 96-103.
- 376 24. Pinchas, S., Intramolecular hydrogen bonding in o-nitrobenzaldehyde and related compounds. *The Journal of*  
377 *Physical Chemistry* **1963**, *67* (9), 1862-1865.
- 378 25. Jezierska-Mazzarello, A.; Szatyłowicz H Fau - Krygowski, T. M.; Krygowski, T. M., Interference of H-  
379 bonding and substituent effects in nitro- and hydroxy-substituted salicylaldehydes. *Journal of Molecular*  
380 *Modeling* **2012**, *18* (0948-5023), 127-135.
- 381 26. Lampert, H.; Mikenda, W.; Karpfen, A., Intramolecular Hydrogen Bonding in 2-Hydroxybenzoyl  
382 Compounds: Infrared Spectra and Quantum Chemical Calculations. *The Journal of Physical Chemistry*  
383 **1996**, *100* (18), 7418-7425.
- 384 27. Meisl, G.; Kirkegaard, J. B.; Arosio, P.; Michaels, T. C. T.; Vendruscolo, M.; Dobson, C. M.; Linse, S.;  
385 Knowles, T. P. J., Molecular mechanisms of protein aggregation from global fitting of kinetic models. *Nature*  
386 *Protocols* **2016**, *11* (2), 252-272.
- 387 28. Leira-Iglesias, J.; Tassoni, A.; Adachi, T.; Stich, M.; Hermans, T. M., Oscillations, travelling fronts and  
388 patterns in a supramolecular system. *Nature Nanotechnology* **2018**, *13* (11), 1021-1027.
- 389 29. Wanzke, C.; Jussupow, A.; Kohler, F.; Dietz, H.; Kaila, V. R. I.; Boekhoven, J., Dynamic Vesicles Formed  
390 By Dissipative Self-Assembly. *ChemSystemsChem* **2020**, *2* (1), e1900044.
- 391 30. Boekhoven, J.; Hendriksen, W. E.; Koper, G. J. M.; Eelkema, R.; van Esch, J. H., Transient assembly of  
392 active materials fueled by a chemical reaction. *Science* **2015**, *349* (6252), 1075.
- 393 31. Singh, N.; Formon, G. J. M.; De Piccoli, S.; Hermans, T. M., Devising Synthetic Reaction Cycles for  
394 Dissipative Nonequilibrium Self-Assembly. *Advanced Materials* **2020**, *32* (20), 1906834.
- 395 32. Deng, J.; Walther, A., ATP-powered molecular recognition to engineer transient multivalency and self-  
396 sorting 4D hierarchical systems. *Nature Communications* **2020**, *11* (1), 3658.

